

## Direct observation of photonic Fermi surfaces by plasmon tomography

C. J. Regan,<sup>1,2</sup> A. Krishnan,<sup>3</sup> R. Lopez-Boada,<sup>4</sup> L. Grave de Peralta,<sup>2,5</sup> and A. A. Bernussi<sup>1,2,a)</sup>

<sup>1</sup>Department of Electrical and Computer Engineering, Texas Tech University, Lubbock, Texas 79409, USA

<sup>2</sup>Nano Tech Center, Texas Tech University, Lubbock, Texas 79409, USA

<sup>3</sup>Department of Electrical Engineering, IIT Madras, Chennai, Tamil Nadu 600036, India

<sup>4</sup>Department of Natural Science, Health and Wellness, Wolfson Campus, Miami Dade College, Miami, Florida 33132, USA

<sup>5</sup>Department of Physics, Texas Tech University, Lubbock, Texas 79409, USA

(Received 7 January 2011; accepted 31 March 2011; published online 14 April 2011)

Light propagation in dielectric plasmonic crystals with different parameters and symmetries was investigated by plasmon tomography. We show that the photonic Fermi surfaces at the crystal's reciprocal lattice space can be observed directly from the Fourier plane images. Directional gaps were observed where the isofrequency wavevectors of the propagating surface plasmon mode intersect the first Brillouin zone of the plasmonic crystal structures. We determined that the angular magnitude of the directional gaps depends strongly on the crystal symmetry and the lattice period. © 2011 American Institute of Physics. [doi:10.1063/1.3581050]

Light generation and manipulation in the nanoscale is a fundamental requirement to achieve ultra-compact passive and active photonic devices for different applications. A major obstacle confronting further miniaturization of dielectric-based photonic devices is the diffraction limit of the light. Surface plasmon polaritons (SPPs) has been considered a promising alternative solution to overcome this issue.<sup>1</sup> Among the various proposed SPP structures, plasmonic crystals are of particular importance. Multiple functionalities can be achieved with a single or combinations of plasmonic crystals. These include sensing, light guiding, splitting, filtering, multiplexing, and realization of subwavelength optical cavities. Predicting, understanding, and experimentally determining the bandgap formation in plasmonic crystals are thus of great importance to achieve the desired device functionality and performance. The formation of bandgaps in plasmonic crystals has been primarily investigated using point-by-point measurements over the first Brillouin zone (FBZ) at different frequencies<sup>2,3</sup> and it has been predicted using sophisticated simulations, which are typically, in both cases, time consuming processes. Consequently simple and alternative approaches to predict and experimentally determine the bandgaps in plasmonic crystals is needed.

In this paper we investigate light propagation in plasmonic crystals using the plasmon tomography technique.<sup>4,5</sup> Using the SPP-coupled leakage radiation, this approach allows for direct imaging of the SPP propagation at the crystal reciprocal space. We found that this method is particularly useful in the analysis of directional gaps in plasmonic crystals with different lattice parameters and symmetries. Similarly to the photonic crystal counterpart, the observed gaps correspond to directions where light propagation is not allowed (directional stopbands).<sup>6</sup> We demonstrate that the directions of allowed propagation in the plasmonic crystals can be predicted by a simple approach based on the location of the photonic Fermi surfaces with respect to the FBZ and the period of the crystal lattice.

Dielectric plasmonic crystals investigated here consist of periodic arrays of air holes defined on 150 nm thick dye-doped polymethylmethacrylate (PMMA) using electron-beam lithography technique. The PMMA layer was doped with Rhodamine 6G, with peak emission at  $\sim 568$  nm wavelength, which was spun over a 50 nm thick gold film deposited on a glass substrate. Figure 1(a) shows the schematic of a plasmonic crystal with square lattice symmetry. In order to verify the fabrication procedures, and to be able to image the plasmonic crystals, the samples were covered with a thin layer of gold and a liftoff step was used to define the corresponding features. A representative scanning electron microscope (SEM) image of a plasmonic crystal with hexagonal symmetry with 200 nm hole diameter and 300 nm period is shown in Fig. 1(b). In this case the image consists of gold pillars over a gold layer. These extra deposition and liftoff steps were solely used for imaging purposes. We fabricated plasmonic crystals with square and hexagonal lattice symmetries with hole diameter ( $d$ ) and lattice period ( $p$ ) varying from 100 nm to 300 nm and from 150 nm to 500 nm, respectively. The samples were investigated by plasmon tomography technique and the Fourier plane (FP) images were obtained using as the excitation source a 532 nm wavelength pump laser. Details of the experimental arrangement can be found in Refs. 4 and 5.

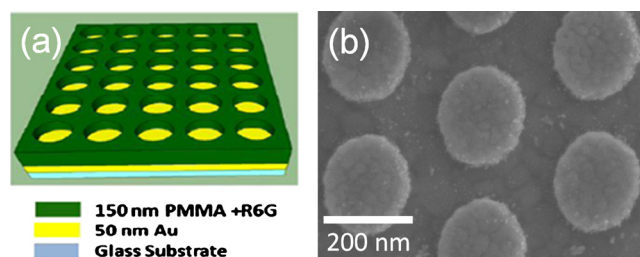


FIG. 1. (Color online) (a) Schematic (not to scale) of fabricated dielectric plasmonic crystal with square lattice symmetry. (b) SEM image of fabricated crystal (hexagonal lattice symmetry) with  $d=200$  nm and  $p=300$  nm, after the extra deposition and liftoff steps for SEM imaging purposes.

<sup>a)</sup>Electronic mail: ayrton.bernussi@ttu.edu.

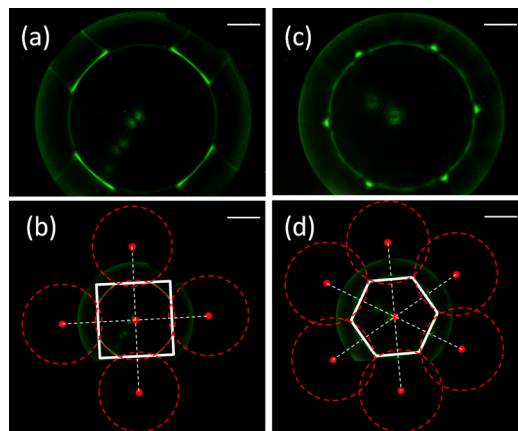


FIG. 2. (Color online) FP images of (a) square ( $d=200$  nm and  $p=300$  nm) and (c) hexagonal ( $d=200$  nm and  $p=350$  nm) plasmonic crystals. Photonic Fermi surfaces (dashed circles) centered at the reciprocal lattice points (thick dots), orthogonal bisection lines (light dashed lines), and FBZ zone (thick continuous lines) of the same square (b) and hexagonal (d) plasmonic crystals. Scale bars correspond to  $5 \mu\text{m}^{-1}$  in (a) and (c) and  $10 \mu\text{m}^{-1}$  in (b) and (d).

Figures 2(a) and 2(c) show FP tomography images of plasmonic crystals with square ( $d=200$  nm and  $p=300$  nm) and hexagonal ( $d=200$  nm and  $p=350$  nm) lattice symmetries, respectively. In these images the thin inner circular ring corresponds to the guided wave plasmon-coupled propagation mode with radius proportional to the magnitude of the wavevector  $k_{spp}=2\pi n_{eff}/\lambda$ , where  $\lambda$  is the wavelength in the freespace and  $n_{eff}$  is the effective refractive index of the plasmon mode.<sup>6</sup> The larger outer weak disk background corresponds to the high numerical aperture (NA=1.49) of the collecting objective lens used in our experiments.<sup>5</sup> The ratio of the diameter of the ring to the diameter of the disk is therefore equal to the ratio of the effective index of the propagating mode to the NA of the collecting microscope objective. Using this approach the effective index for the modes in each crystal can be calculated as 1.017, 1.019, 1.024, 1.040, 1.064, 1.072 for Figs. 3(a)–3(f), respectively. Similarly, the magnitude of the real part of the wavevectors for the modes in each crystal can be calculated as  $11.250 \mu\text{m}^{-1}$ ,  $11.272 \mu\text{m}^{-1}$ ,  $11.327 \mu\text{m}^{-1}$ ,  $11.504 \mu\text{m}^{-1}$ ,  $11.770 \mu\text{m}^{-1}$ , and  $11.858 \mu\text{m}^{-1}$ , for Figs. 3(a)–3(f), respectively. The increase in effective index (and thus wavenumber) can be seen in terms of increasing proportion of PMMA to air covering the gold film as the period of holes increases for the same hole size. The inner rings shown in Figs. 2(a) and 2(c) are reminiscent of the constant energy circle (Fermi surface), or isofrequency dispersion relation, observed in crystalline structures commonly studied in solid state physics,<sup>7</sup> and thus we refer here as *photonic Fermi surface*. The bright arc segments superimposed to the inner ring in Fig. 2(a) indicate that light propagation in the plasmonic crystal with square lattice symmetry can only occur in certain preferential directions which are determined by the four arcs and with a beam propagation divergence determined by the length of the arc segments.<sup>8</sup> A similar result can be also verified in Fig. 2(c) where light propagation only occurs at preferential directions specified by the hexagonal lattice symmetry. However, the significantly reduced arc segment lengths observed in Fig. 2(c) indicate very small beam propagation divergence, or a high degree of beam direction-

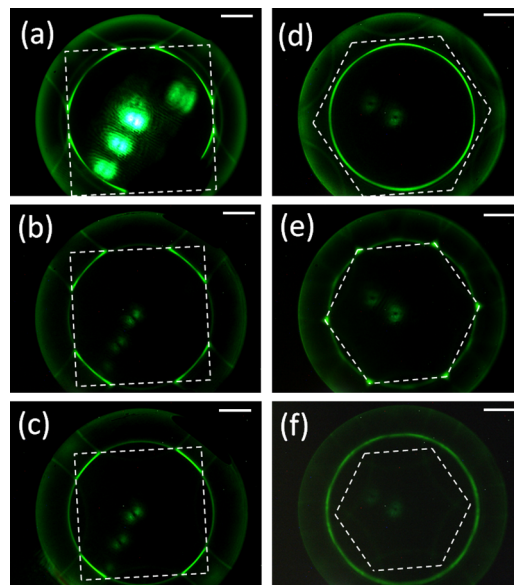


FIG. 3. (Color online) FP images of the photonic Fermi surfaces and corresponding FBZ for plasmonic crystals with fixed hole diameter  $d=200$  nm and different periods. Square lattice symmetry: (a)  $p=280$  nm, (b)  $p=320$  nm, and (c)  $p=300$  nm, and hexagonal lattice symmetry: (d)  $p=350$  nm, (e)  $p=350$  nm, and (f)  $p=400$  nm. Scale bars correspond to  $5 \mu\text{m}^{-1}$ .

ality, for this particular combination of lattice symmetry, air hole diameter, and lattice period.

In analogy to electrons in solid state crystals, the intersecting weak rings displaced from the center of the inner ring [see Figs. 2(a) and 2(c)] correspond to direct images of the photonic Fermi surfaces centered at each reciprocal lattice point, with center-to-center separation determined by the lattice vectors.<sup>6</sup> In order to support this statement we show in Figs. 2(b) and 2(d) the reciprocal lattice points for the same samples used to obtain Figs. 2(a) and 2(c), respectively. In this case, each reciprocal lattice point is separated by the lattice vector  $G=2\pi/p$ , where  $p$  is the period of each lattice in the real space. The photonic Fermi surfaces shown in Figs. 2(b) and 2(d) are centered at each point of the reciprocal lattice with radius equal to  $k_{spp}$ . In our analysis, only the first nearest neighbors were considered. An excellent correspondence between the photonic Fermi surfaces centered at the reciprocal lattice points and the rings displaced from the central ring is evident in Figs. 2(b) and 2(d). The FBZ can then be determined at the intersecting region defined by perpendicular bisection lines between an origin reference (center of the inner ring) and the nearest neighbors. As shown in Figs. 2(b) and 2(d) the gaps in the isofrequency dispersion ring only occur when the ring corresponding to the wavevector  $k_{spp}$  crosses the boundaries of the FBZ, with allowed propagation existing within the FBZ and forbidden gaps occurring outside the FBZ. The approach used to determine the FBZ is particularly simple and advantageous since it does not require time consuming and sophisticated simulation methods, or point-by-point experiential procedures, to predict the dispersion relation in plasmonic crystals.<sup>6</sup>

In order to effectively design the desired directional gaps it is instructive to examine the dependence of the gaps on both the hole size and the lattice period. Figure 3 shows FP tomography images of plasmonic crystals with square [Figs. 3(a)–3(c)] and hexagonal symmetries [Figs. 3(d)–3(f)] with a

fixed hole diameter ( $d=200$  nm) but different lattice periods. The FBZ is also shown in Fig. 3 for each plasmonic crystal. It is evident from Fig. 3 that the period has a strong influence on the angular gap width. When the period is increased, for all structures showing the gaps, the width of the FBZ decreases, leading to less area inside the FBZ and thus to higher propagation directivity and larger gap widths. The regions where the FBZ do not cross the propagating wavevector there is clearly no directional gaps opened in the dispersion curve [Figs. 3(d) and 3(f)]. There is also, however, a much weaker dependence on the hole diameter (not shown here). We determined that when  $d < 190$  nm no gaps were observed for any crystal period and symmetry. However, small changes in the gap width were observed for  $d > 190$  nm. This is attributed to a decrease in the effective refractive index of the plasmon mode as the air hole diameter increases (similar to the changes in wavenumber discussed above). Consequently, the magnitude of the wavevector  $k_{spp}$  is reduced, resulting in photonic Fermi surfaces with smaller diameter which in turn modifies the intersection positions with the FBZ. Figures 3(d)–3(f) also show why hexagonal lattice symmetry is preferred for designing complete band-gap structures: the FBZ in the hexagonal symmetry resembles more closely to a circle [see Fig. 3(e)] such that the defined region will almost completely overlap with the propagating mode in all directions.<sup>9</sup> As shown in Fig. 3, an appropriate choice of the plasmonic crystal parameters can result in highly directional passbands [see Fig. 3(e)]. This can be particularly useful for beam collimation and sensing applications, where small changes in the effective refractive index of the plasmon coupled mode would result in pronounced changes in beam directivity.

In summary, we have investigated the dispersion characteristics of dielectric plasmonic crystals using FP plasmon tomography. Well-defined directional stopbands were clearly observed in the FP images of the fabricated structures. We determined that the angular magnitude of the directional gaps strongly depends on the crystal symmetry and the lattice period. We have introduced a simple, but effective, method to determine and predict the magnitude of these gaps, through intersection between the coupled surface plasmon isofrequency dispersion ring and the FBZ. We have shown that a careful choice of plasmonic crystal characteristics and symmetry can result in high propagation directivity. This has strong potential for generating high in-plane collimated beams and for sensing applications.

This work was partially supported by the NSF CAREER (Award No. ECCS-0954490), U.S. Army CERDEC (Contract No. W15P7T-07-D-P040), and by the J. F. Maddox Foundation.

- <sup>1</sup>W. L. Barnes, A. Dereux, and T. W. Dereux, *Nature (London)* **424**, 824 (2003).
- <sup>2</sup>L. Feng, M. H. Lu, V. Lomakin, and Y. Fainman, *Appl. Phys. Lett.* **93**, 231105 (2008).
- <sup>3</sup>S. C. Kitson, W. L. Barnes, and J. R. Sambles, *Phys. Rev. Lett.* **77**, 2670 (1996).
- <sup>4</sup>S. P. Frisbie, C. F. Chesnutt, M. E. Holtz, A. Krishnan, L. Grave de Peralta, and A. A. Bernussi, *IEEE Photonics Journal* **1**, 153 (2009).
- <sup>5</sup>L. Grave de Peralta, R. Lopez-Boada, A. Ruiz-Columbie, S. Park, and A. A. Bernussi, *J. Appl. Phys.* **109**, 023101 (2011).
- <sup>6</sup>A. Giannattasio and W. L. Barnes, *Opt. Express* **13**, 428 (2005).
- <sup>7</sup>A. A. Kordyuk, S. V. Borisenko, M. S. Golden, S. Legner, K. A. Nenkov, M. Knupfer, J. Fink, H. Berger, L. Forro, and R. Follath, *Phys. Rev. B* **66**, 014502 (2002).
- <sup>8</sup>J. Y. Lalue, A. Drezet, C. Genet, and T. W. Ebbesen, *New J. Phys.* **10**, 105014 (2008).
- <sup>9</sup>P. R. Villeneuve and M. Piché, *Phys. Rev. B* **46**, 4973 (1992).